This paper is published as part of a PCCP Themed Issue on:
Electronic Structures and Reaction Dynamics of Open-shell Species

Guest Editors:
Jingsong Zhang - *University of California, Riverside*
Martin Head-Gordon - *University of California, Berkeley*

Editorial

Electronic Structures and Reaction Dynamics of Open-shell Species

Phys. Chem. Chem. Phys., 2009 **DOI:** 10.1039/b909815c

Communication

Observation of organosulfur products (thiovinoxy, thioketene and thioformyl) in crossed-beam experiments and low temperature rate coefficients for the reaction S(^{1}D) + C_2H_4

Francesca Leonori, Raffaele Petrucci, Nadia Balucani, Piergiorgio Casavecchia, Marzio Rosi, Coralie Berteloite, Sébastien D. Le Picard, André Canosa and Ian R. Sims, *Phys. Chem. Chem. Phys.*, 2009

DOI: 10.1039/b900059c

Papers

A crossed molecular beams study of the reaction of the ethynyl radical ($C_2H(X^2\Sigma^+)$) with allene ($H_2CCCH_2(X^1A_1)$)

Fangtong Zhang, Seol Kim and Ralf I. Kaiser, *Phys. Chem. Chem. Phys.*, 2009

DOI: 10.1039/b822366a

Effects of reactant rotational excitation on H + O_2 → OH + O reaction rate constant: quantum wave packet, quasi-classical trajectory and phase space theory calculations

Shi Ying Lin, Hua Guo, György Lendvay and Daiqian Xie, *Phys. Chem. Chem. Phys.*, 2009

DOI: 10.1039/b822746m

Quasiclassical trajectory calculations of the HO_2 + NO reaction on a global potential energy surface

Chao Chen, Benjamin C. Shepler, Bastiaan J. Braams and Joel M. Bowman, *Phys. Chem. Chem. Phys.*, 2009

DOI: 10.1039/b823031e

A companion perturbation theory for state-specific multireference coupled cluster methods

Francesco A. Evangelista, Andrew C. Simmonett, Henry F. Schaefer III, Debashis Mukherjee and Wesley D. Allen, *Phys. Chem. Chem. Phys.*, 2009

DOI: 10.1039/b822910d

On the vibronic level structure in the NO_3 radical
Part III. Observation of intensity borrowing *via* ground state mixing

John F. Stanton and Mitchio Okumura, *Phys. Chem. Chem. Phys.*, 2009

DOI: 10.1039/b902252j

The photoelectron spectrum of CCl_2^-: the convergence of theory and experiment after a decade of debate

Scott W. Wren, Kristen M. Vogelhuber, Kent M. Ervin and W. Carl Lineberger, *Phys. Chem. Chem. Phys.*, 2009

DOI: 10.1039/b822690c

Predissociation of the $A^2\Sigma^+$ ($v' = 3$) state of the OH radical

Dragana Ćirić Radenović, André J. A. van Roij, Shiou-Min Wu, J. J. ter Meulen, David H. Parker, Mark P. J. van der Loo and Gerrit C. Groenenboom, *Phys. Chem. Chem. Phys.*, 2009

DOI: 10.1039/b900249a

Ultraviolet photodissociation of the SD radical in vibrationally ground and excited states

Xianfeng Zheng, Jingze Wu, Yu Song and Jingsong Zhang, *Phys. Chem. Chem. Phys.*, 2009

DOI: 10.1039/b900332k

Correlated fine structure branching ratios arising from state-selected predissociation of ClO ($A^2\Pi_{3/2}$)

Kristin S. Dooley, Michael P. Grubb, Justine Geidosch, Marloes A. van Beek, Gerrit C. Groenenboom and Simon W. North, *Phys. Chem. Chem. Phys.*, 2009

DOI: 10.1039/b823004h

Photodissociation of heptane isomers and relative ionization efficiencies of butyl and propyl radicals at 157 nm

Ruchira Silva, Wilson K. Gichuhi, Michael B. Doyle, Alexander H. Winney and Arthur G. Suits, *Phys. Chem. Chem. Phys.*, 2009

DOI: 10.1039/b823505h

Correlated fine structure branching ratios arising from state-selected predissociation of ClO ($A\ ^2\Pi_{3/2}$)

Kristin S. Dooley,[a] Michael P. Grubb,[a] Justine Geidosch,[a] Marloes A. van Beek,[b] Gerrit C. Groenenboom[b] and Simon W. North*[a]

Received 23rd December 2008, Accepted 15th April 2009
First published as an Advance Article on the web 29th April 2009
DOI: 10.1039/b823004h

We have extended our investigation of the v'-dependent predissociation dynamics of the ClO $A\ ^2\Pi_{3/2}$ state using velocity-map ion imaging. Correlated fine-structure branching ratios are reported for $v' = 0$–5. The measured branching ratios are non-statistical and are qualitatively inconsistent with adiabatic dissociation dynamics. The coupling constants between the $A\ ^2\Pi_{3/2}$ state and several dissociative excited state potentials have been optimized, as have the locations of the crossing points, based on comparison to previously reported v'-dependent predissociation rates. Using these optimized potentials we have modeled the branching ratios in the diabatic limit but the lack of agreement with experiments suggests the importance of exit channel coupling. Coupled channel calculations including 9 coupled potentials provide modest improvement with experiment but differences remain.

I. Introduction

It is well established that halogen oxides are important intermediates in the catalytic destruction of stratospheric ozone.[1–3] These species are also ideal benchmark systems for open-shelled photodissociation dynamics, particularly the comparison of experiment and theory, for several reasons; their electronic spectroscopy is well studied, both atomic fragments can be probed using state-selective ionization, and diatomic molecules are amenable to interrogation using high-level *ab initio* theory. A recent study of the state-selected photodissociation of OH ($A\ ^2\Sigma^+$) highlights the progress in describing such systems.[4,5]

The electronic spectroscopy of ClO, in particular transitions between the bound $X\ ^2\Pi_{3/2}$ and $A\ ^2\Pi_{3/2}$ states, has been well studied.[6–10] Vibronic transitions to bound levels of the $A\ ^2\Pi_{3/2}$ state are responsible for resolved bands at wavelengths between 316 nm and the dissociation threshold at 263.01 ± 0.01 nm. At wavelengths shorter than 263 nm the spectrum is characterized by a broad continuum that terminates near 220 nm, a manifestation of the continuity of the Franck–Condon intensity involving the $A\ ^2\Pi_{3/2}$ state. There have been two recent *ab initio* investigations of the ClO excited state potentials. Lane *et al.* employed large Dunning basis sets and the complete active space self-consistent field (CASSCF) method to calculate the ground and excited state potentials of ClO.[11] In an independent study, Toniolo *et al.* used a multiconfigurational SCF plus CI method to calculate the ClO excited states.[12] A focus of both studies was understanding the origin modeling of the vibrational-dependent predissociation rates of the $A\ ^2\Pi$ state.

There have been several recent experimental studies of ClO photodissociation in the continuum region,[13–15] near the $O(^1D)$ threshold,[15–17] and below the $O(^1D)$ threshold.[15,18] Most of these studies focused on assessing the relative importance of the $O(^1D)$ and $O(^3P)$ product channels. Below the dissociation threshold of the $A\ ^2\Pi_{3/2}$ state, there are six correlated fine-structure states that are energetically accessible:

$$ClO(X\ ^2\Pi_{3/2}) \rightarrow ClO(A\ ^2\Pi_{3/2}) \rightarrow Cl(^2P_{3/2}) + O(^3P_2) \quad (1)$$

$$\rightarrow Cl(^2P_{3/2}) + O(^3P_1) \quad (2)$$

$$\rightarrow Cl(^2P_{3/2}) + O(^3P_0) \quad (3)$$

$$\rightarrow Cl(^2P_{1/2}) + O(^3P_2) \quad (4)$$

$$\rightarrow Cl(^2P_{1/2}) + O(^3P_1) \quad (5)$$

$$\rightarrow Cl(^2P_{1/2}) + O(^3P_0) \quad (6)$$

Recently Kim *et al.* examined the v'-dependent predissociation of ClO below the $O(^1D)$ threshold and reported product state branching ratios for the six asymptotic channels.[18] Although fine-structure distributions averaged over the coincident fragment state provide considerable insight, the correlated fine-structure distributions are often far more revealing. The observed correlated branching ratios measured by Kim *et al.* were non-statistical and highly dependent on the initial $A\ ^2\Pi_{3/2}$ vibrational state ($v' = 6$–11). Such measurements reflect not only the coupling of the $A\ ^2\Pi_{3/2}$ state to dissociative states in the Franck–Condon region (the crossing region) but also coupling between the dissociative states at longer internuclear separation (the recoupling zone). Initial analysis indicated that the fine-structure branching was more consistent with the diabatic (sudden) limit than the adiabatic limit using the couplings in the Franck–Condon region derived from the work of Lane *et al.*[11] to calculate initial state populations. However, there were significant differences between the diabatic prediction and experiment suggesting errors in the

[a] *Department of Chemistry, Texas A&M University, P. O. Box 30012, College Station, Texas, 77842, USA. E-mail: swnorth@tamu.edu; Fax: +1 (1)979 845 2971*
[b] *Theoretical Chemistry, Institute for Molecules and Materials, Radboud University Nijmegen, Heyendaalseweg 135, 6525 AJ, Nijmegen, The Netherlands*

initial coupling and/or dynamical effects in the exit channel. In the present paper we extend the experimental work of Kim *et al.* to lower vibrational levels of the $A\ ^2\Pi_{3/2}$ state ($v' = 0$–5) and expand the analysis of Lane *et al.* to include additional predissociative states and optimization of the potentials. The expanded analysis was pursued to demonstrate that the differences between the diabatic model and experiment must be due to exit channel couplings. In addition, coupled channel calculations provide modest improvements in comparison to experiment and highlight the remaining challenges.

II. Experiment

The velocity-map ion-imaging apparatus employed in the present experiments has been described in detail elsewhere.[15,19] Briefly, a pulsed molecular beam of ClO seeded in He and collimated by a conical skimmer was intersected at 90° by two co-propagating linearly polarized laser beams. The photolysis beam (285–310 nm) was generated by a Nd-YAG (Spectra Physics GCR 150-10) pumped dye laser (Spectra Physics PDL-1) with output frequency doubling by a Spectra Physics WEX-1. The fundamental wavelength output was calibrated using a Ne–Cu hollow cathode lamp and a double-Fresnel rhomb and a polarizer were used to ensure vertical polarization of the beam. The oxygen atoms [$O(^3P_{2,1,0})$] were state-selectively probed using 2 + 1 REMPI transitions near 226 nm ($3p\ ^3P_{2,1,0} \leftarrow 2p\ ^3P_{2,1,0}$).[20] These wavelengths were generated by an Nd-YAG (Spectra Physics GCR 150-10) pumped dye laser (LAS LDL 2051) whose output was frequency doubled using a BBO crystal. An assembly of four Pellin–Broca prisms was used to ensure consistent overlap of the dissociation and probe laser beams during REMPI scans. The probe beam was delayed with respect to the photolysis beam by approximately 20 ns. Typical photolysis and probe pulse energies were 20 μJ and 30 μJ, respectively. We observed no evidence for multiphoton dissociation and the resulting fragment speeds are consistent with a single photon process. The oxygen ions were accelerated using velocity-mapping ion optics[21–23] down a 50 cm long field-free flight tube along the same axis as the molecular beam. At the end of the flight tube the ions strike a position sensitive detector consisting of a dual microchannel plate (MCP)-phosphor screen assembly. Images were acquired using a CCD camera and collected using a frame-grabber and the IMAQS software of Suits and co-workers.[23] An off-axis photomultiplier tube was used to monitor the total ion signal for 2 + 1 REMPI scans and ensure correct gating of the MCP detector. Final images for each of the probed oxygen states were collected as the probe laser was repeatedly scanned across the fragment Doppler profile. The 3-dimensional velocity distributions were then reconstructed from the 2-dimensional projections using both the BASEX[24] and pBASEX[25] programs.

The molecular beam of ClO was formed by the flash pyrolysis of Cl_2O–He mixture. The Cl_2O was synthesized *in vacuo* by the method of Cady[26] and was kept at −78 °C to provide an approximately 5% mix in 1 atm of He. The Cl_2O–He sample was introduced into the instrument through a commercially available pulsed valve (Parker Hannifin Series 9) fit with a pyrolytic nozzle assembly. The active region of the nozzle assembly consisted of a 3 cm long alumina tube wrapped in nickel–chromium alloy wire allowing the tube to be resistively heated to 800 K. The molecular beam was modestly cooled as it passed through a water-cooled endcap before expanding into the chamber. Based on images taken near the threshold for $O(^1D)$ production from ClO[15] under identical conditions we estimate that the ClO radicals can be characterized by $T_{rot} < 100$ K, $T_{vib} < 200$ K, and $T_{elec} < 200$ K. We note, however, that an accurate characterization rotational temperature is not critical in current studies since the photodissociation laser selects a narrow range of rotational states of the $\Omega = 3/2$ spin–orbit component of the bound A-state. We observed no evidence of Cl_2O photodissociation in the $O(^3P_J)$ images since O atoms cannot arise from single photon dissociation, and the fact that any O-atom contribution from Cl_2O would yield a broad speed distribution which can be easily distinguished from the sharp ClO photodissociation features.

III. Results and discussion

A Experimental measurements

Fig. 1 shows typical $O(^3P_{0,1,2})$ ion images (left) and reconstructions (right) arising from ClO photodissociation at 299.50 nm corresponding to the bandhead region of the $v' = 4$ level of the $A\ ^2\Pi_{3/2}$ state. As previously noted, it is possible to resolve the contributions from $Cl(^2P_{3/2})$ and $Cl(^2P_{1/2})$ formed in

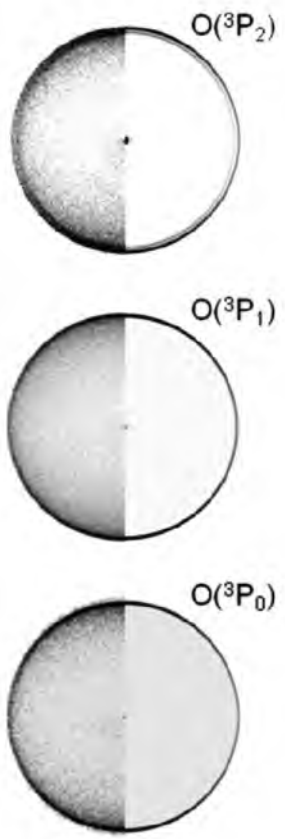

Fig. 1 Raw $O(^3P_J)$ images (left panels) and reconstructed images (right panels) arising from ClO photodissociation at 299.50 nm.

coincidence with each probed oxygen fine-structure state. The two rings evident in the $O(^3P_2)$ image correspond to the formation of coincident $Cl(^2P_{3/2})$ and $Cl(^2P_{1/2})$ fragments. The single ring observed in the $O(^3P_1)$ and $O(^3P_0)$ images indicate that these states are only formed in coincidence with $Cl(^2P_{3/2})$. Forward convolution fitting (solid line) of the speed distributions permits an accurate measurement of the $Cl(^2P_{3/2})/Cl(^2P_{1/2})$ branching ratio for each $O(^3P_J)$ fragment. These ratios are highly reproducible, with an estimated error of less than 3%. Once the $Cl(^2P_{3/2})/Cl(^2P_{1/2})$ branching ratio has been determined for each oxygen fine-structure state the correlated fine-structure branching ratios for each vibrational level probed are obtained by including the weighting of each oxygen state based on the integrated 2 + 1 REMPI signals.[20]

Table 1 shows the experimental correlated branching ratios measured in this study for $v' = 0$–5 and includes previous data from ref. 18 (in bold). Uncertainty in the experimental branching ratios is dominated by determination of the oxygen fine-structure ratio. We observe that the $O(^3P_2)$ signal is affected by a small amount of probe laser background which was minimized by employing low probe laser power. Based on multiple measurements, we find that the $O(^3P_2)/O(^3P_1)/O(^3P_0)$ ratio for a given v' state is very reproducible and we estimate that the uncertainty for this ratio is approximately 10%. In contrast, the $Cl(^2P_{3/2})/Cl(^2P_{1/2})$ branching derived from a single oxygen state are very robust with errors of less than 3%. It should be noted that we assume that experimental branching ratios for each vibrational state are independent of J'. Howie *et al.* observed no evidence of J'-dependent predissociation indicating that the primary interaction of the dissociative states with the $A\ ^2\Pi_{3/2}$ state is *via* spin–orbit coupling.[10] In addition, the J'-dependence of the correlated state branching ratios was explicitly examined by Kim *et al.* for the $v' = 6$ and $v' = 10$ bands. No change in correlated state branching ratios was observed as the photolysis laser was tuned from the bandhead to higher J'-states.[18] There are several immediate conclusions that can be reached from even a cursory analysis of the experimental branching data. First, by inspection the results are inconsistent with a statistical (strong coupling) limit and exhibit a clear v' = dependence. Second, the results are inconsistent with adiabatic dynamics which does not predict the number of asymptotic channels that are observed in the experiment. This is in agreement with previous photodissociation experiments above the $O(^1D)$ threshold. In these experiments dissociation originating from excitation to the continuum of the $A\ ^2\Pi$ state, based on an observed parallel anisotropy parameter (*i.e.* a parallel transition), resulted in only a minor yield of $O(^3P_J)$ fragments suggesting little curve crossing. Finally, the $Cl(^2P_{1/2}) + O(^3P_0)$ channel, despite being energetically accessible, is not observed at any wavelength.

The spatial anisotropy of the photofragments can be described using the following equation,

$$I(\theta) = \tfrac{1}{4\pi}[1 + \beta P_2(\cos\theta)] \,, \qquad (7)$$

where $P_2(\cos\theta)$ is the second Legendre polynomial, θ is the angle between the laser polarization direction and the fragment recoil, and β is the anisotropy parameter. In the limit of axial recoil for a diatomic molecule $\beta = 2$ for a purely parallel transition ($\Delta\Omega = 0$) and $\beta = -1$ for a purely perpendicular transition ($\Delta\Omega = \pm 1$). The present experiments involve the $X\ ^2\Pi_{3/2}$–$A\ ^2\Pi_{3/2}$ parallel transition ($\Delta\Omega = 0$) corresponding to an intrinsic anisotropy parameter of $\beta = 2$. We observe no differences, *i.e.* with the mutual error bounds, between the spatial anisotropies of individual $O(^3P_J)$ images at a given photolysis wavelength. This is consistent with a common origin for the products and suggests that fragment orbital alignment is not significantly influencing the measured signals. However, we observe anisotropy parameters less than the limiting value for all ClO data collected. Since the $O(^3P_0)$ fragment has no angular momentum the measured ion images for this fragment reflect only the spatial anisotropy. For the $v' = 4$ image shown in Fig. 1, the $O(^3P_0)$ is best fit by an anisotropy parameter of $\beta = 0.65 \pm 0.10$. A recent study provides a method to evaluate photofragment spatial anisotropy as a function of excitation frequency, dissociative state lifetime, and the rotational structure.[27,28] We find that the

Table 1 Correlated fine-structure branching ratios from ClO photodissociation. The bold values are from experiment and bold italic values exceed the limits of the diabatic model

Atomic States	$v' = 0$	$v' = 1$	$v' = 2$	$v' = 3$	$v' = 4$	$v' = 5$	$v' = 6$	$v' = 7$	$v' = 8$	$v' = 9$	$v' = 10$	$v' = 11$
$Cl(^2P_{3/2}) + O(^3P_2)$	**0.10**	**0.07**	**0.24**	**0.26**	**0.21**	**0.28**	**0.19**	**0.22**	**0.09**	**0.29**	**0.24**	**0.19**
Coupled channel:	0.35	0.34	0.33	0.30	0.28	0.24	0.25	0.32	0.26	0.30	0.26	0.28
Diabatic:	0.17	0.18	0.22	0.23	0.22	0.26	0.27	0.22	0.24	0.22	0.25	0.17
$Cl(^2P_{1/2}) + O(^3P_2)$	***0.37***	**0.31**	***0.37***	**0.09**	**0.12**	**0.08**	**0.18**	**0.02**	**0.10**	**0.18**	**0.26**	**0.31**
Coupled channel:	0.20	0.18	0.20	0.18	0.19	0.14	0.13	0.22	0.12	0.23	0.11	0.12
Diabatic:	0.21	0.20	0.19	0.22	0.20	0.25	0.28	0.20	0.22	0.19	0.23	0.13
$Cl(^2P_{3/2}) + O(^3P_1)$	**0.37**	***0.56***	**0.29**	***0.41***	**0.35**	**0.22**	**0.15**	**0.19**	**0.24**	**0.17**	**0.21**	**0.37**
Coupled channel:	0.37	0.39	0.31	0.32	0.30	0.28	0.28	0.31	0.28	0.32	0.30	0.30
Diabatic:	0.29	0.30	0.34	0.31	0.33	0.29	0.28	0.33	0.31	0.33	0.31	0.37
$Cl(^2P_{1/2}) + O(^3P_1)$	**0.10**	**0.00**	**0.07**	**0.00**	**0.00**	**0.16**	**0.22**	***0.34***	**0.21**	***0.30***	**0.16**	**0.00**
Coupled channel:	0.02	0.03	0.02	0.02	0.06	0.11	0.11	0.04	0.11	0.04	0.09	0.09
Diabatic:	0.21	0.19	0.09	0.10	0.09	0.07	0.07	0.10	0.08	0.09	0.08	0.12
$Cl(^2P_{3/2}) + O(^3P_0)$	**0.06**	**0.06**	**0.04**	**0.24**	***0.33***	***0.26***	***0.26***	**0.22**	***0.32***	**0.06**	**0.13**	**0.13**
Coupled channel:	0.06	0.07	0.13	0.17	0.17	0.24	0.24	0.12	0.24	0.11	0.24	0.21
Diabatic:	0.12	0.13	0.17	0.14	0.16	0.13	0.11	0.16	0.15	0.17	0.14	0.20
$Cl(^2P_{1/2}) + O(^3P_0)$	**0.00**	**0.00**	**0.00**	**0.00**	**0.00**	**0.00**	**0.00**	***0.02***	***0.03***	**0.00**	**0.00**	**0.00**
Coupled channel:	0.00	0.00	0.00	0.00	0.00	0.00	0.00	0.00	0.00	0.00	0.00	0.00
Diabatic:	0.00	0.00	0.00	0.00	0.00	0.00	0.00	0.00	0.00	0.00	0.00	0.00

measured anisotropy parameters are well reproduced using the reported spectroscopic information.

B Modeling of the correlated fine-structure distributions

In our initial study on ClO predissociation[18] we employed the 3-state model of Lane *et al.* to calculate the fine-structure branching ratios in the adiabatic and diabatic limits. The significant differences between the experiment and the diabatic limit treatment at the correlated level were attributed to two factors: (i) incorrect coupling of the dissociative potentials to the $A\ ^2\Pi_{3/2}$ state which provides initial weightings of the dissociative potentials for the diabatic analysis; (ii) the neglect of exit channel couplings which can alter the distribution established in the crossing region. Although both of these factors ultimately influence the fine-structure branching ratios, only errors in the coupling in the Franck–Condon region will affect the predissociation rates. Therefore, as a first step in improved modeling of the experimental branching ratios we have re-optimized the dissociative potentials of Lane *et al.*, altering both the locations of the crossings with the $A\ ^2\Pi_{3/2}$ state and the coupling constants, using the experimental predissociation rates as the constraint.[8,10] The BCONT program[29,30] was used to calculate predissociation rates and an optimization code, based on an amoeba algorithm, iteratively adjusted coupling constants between each dissociative state and the $A\ ^2\Pi_{3/2}$ state and floated the crossing point for each dissociative state until the best fit to the experimental rates was obtained. We have used R-independent coupling constants for potentials in BCONT, including the $3\ ^2\Pi$ state despite the strong electrostatic coupling with the $A\ ^2\Pi_{3/2}$ state which should be R-dependent as noted previously.[11]

We find that only four dissociative potentials are required to obtain an acceptable fit to the experimental rates: the $2^4\Sigma^-$, $1^2\Delta$, $1^4\Delta$, and $3^2\Pi$. It should be noted that the $1^4\Delta$ and the $1^4\Sigma^+$ states both cross the $A\ ^2\Pi_{3/2}$ state near $R = 1.95$ Å and thus the relative importance of each state is difficult to assess. We chose to fit only the $1^4\Delta$ state based on the relative $1^4\Delta$ and the $1^4\Sigma^+$ coupling constants reported by Toniolo *et al.*[12] Our derived coupling constant for the $1\ ^4\Delta$ should, therefore, be considered as a sum of the coupling constants for both the $1^4\Delta$ and $1^4\Sigma^+$ states. The inclusion of additional dissociative states beyond the four states employed did not provide significant improvement of the fit. The results of the optimization are shown in Fig. 2 and 3. Fig. 2 illustrates that the final potentials are very close to the initial potentials of Lane *et al.*[11] The largest shift is found for the $1\ ^2\Delta$ state which crosses the $A\ ^2\Pi_{3/2}$ state near the inner wall. The predissociation rates predicted for this potential results in a broad, non-oscillatory, v'-dependence as discussed by Lane *et al.* We find a significant improvement to the fit of the experimental predissociation rate data (Fig. 3) compared to the model of Lane *et al.* which included only the $3\ ^2\Pi$, $1\ ^4\Sigma^+$, and the $2\ ^4\Sigma^-$ dissociative states. The local maximum in the v'-dependent rates coincides with the crossing of $3\ ^2\Pi$ state.[11] The coupling constants between the dissociative states and the $A\ ^2\Pi_{3/2}$ state derived from the optimization are given in Table 2. The *ab initio* coupling constants calculated by Toniolo *et al.* and the derived coupling constants of Lane *et al.* are provided in Table 2 for comparison. Overall there is excellent agreement with the optimized results of Lane *et al.* and purely *ab initio* results of Toniolo *et al.* considering the combined treatment of the $1^4\Delta$ and $1^4\Sigma^+$ states. We do find, however, a lower coupling constant for the $3\ ^2\Pi$ state of approximately 20%. The lower derived coupling constant for this state, whose interaction with the $A\ ^2\Pi_{3/2}$ state is dominated by electrostatic coupling, is consistent with the lack of observed perturbation in the vibronic spectrum. The decrease in the $3\ ^2\Pi$ coupling is a consequence of including the broad v'-dependence

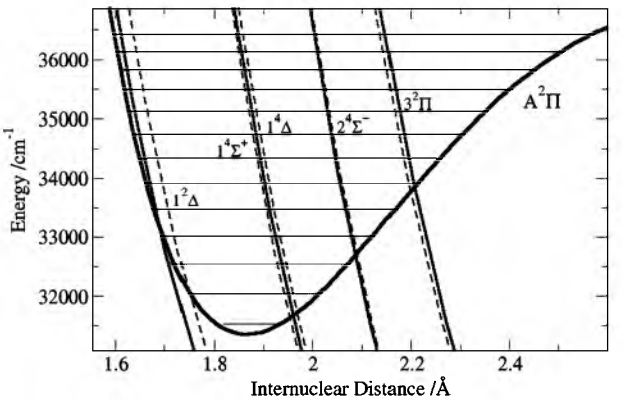

Fig. 2 Excited state potentials for ClO from ref. 11 and the $A\ ^2\Pi_{3/2}$ RKR curve calculated in ref. 10. The $A\ ^2\Pi_{3/2}$ vibrational states are indicated by the horizontal lines and the solid lines represent the results of the optimization described in the text.

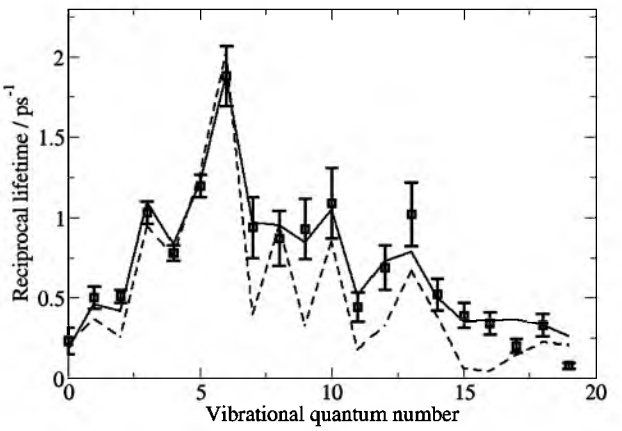

Fig. 3 Experimentally determined v'-dependent predissociation rates of the $A\ ^2\Pi_{3/2}$ state reported in ref. 10 ($v' \leq 7$) and ref. 8 ($v' \geq 8$). The dashed line is the model from ref. 11 and the solid line is the result of the optimization described in the text.

Table 2 Coupling constants between the $A\ ^2\Pi_{3/2}$ state and dissociative electronic states

	Lane *et al.*[11]	Toniolo *et al.*[12]	This work
$1^4\Sigma^+$	49.7 cm^{-1}	13 cm^{-1}	N/A
$2^4\Sigma^-$	82 cm^{-1}	69 cm^{-1}	71.6 cm^{-1}
$3^2\Pi$	125.4 cm^{-1}	124 cm^{-1}	99.2 cm^{-1}
$1^4\Delta$	N/A	28 cm^{-1}	46.5 cm^{-1}
$1^2\Delta$	N/A	57 cm^{-1}	59.9 cm^{-1}

Table 3 Partial contributions of atomic fine-structure states to ClO molecular states as calculated in ref. 18

	ClO molecular states				
Atomic states	$1\ ^4\Sigma^+$	$2\ ^4\Sigma^-$	$3\ ^2\Pi$	$1\ ^2\Delta$	$1\ ^4\Delta$
$Cl(^2P_{3/2}) + O(^3P_2)$	0.2500	0.2778	0.3333	0.1667	0.1667
$Cl(^2P_{1/2}) + O(^3P_2)$	0.3333	0.2778	0.3611	0.1111	0.2222
$Cl(^2P_{3/2}) + O(^3P_1)$	0.2500	0.2778	0.2222	0.3889	0.2778
$Cl(^2P_{1/2}) + O(^3P_1)$	0.0000	0.0556	0.0278	0.1111	0.2222
$Cl(^2P_{3/2}) + O(^3P_0)$	0.1667	0.1111	0.0556	0.2222	0.1111
$Cl(^2P_{1/2}) + O(^3P_0)$	0.0000	0.0000	0.0000	0.0000	0.0000

contribution of the $1\ ^2\Delta$ state and the constraint of matching the predissociation rate maximum at $v' = 6$.

The fine-structure branching ratio for each vibrational state is obtained by multiplying the normalized weighting of each dissociative state, based on the BCONT predissociation rates for each state, by the diabatic matrix (Table 3) which reflects the partial contribution of atomic states to each molecular state.[18,31,32] The fine-structure branching ratios calculated using this procedure are provided in Table 1. We find that the branching calculated from the optimized potentials provide an overall better fit to the experimental data than the original 3-potential model of Lane *et al.* although the improvement is modest. Thus, significant differences remain which must be attributed to exit channel dynamics beyond the Franck–Condon region. Given the complex nature of the observables it is often more instructive to examine alternative representations, in this case summed over coincident fragment populations. The diabatic prediction of the overall v'-dependent $Cl(^2P_{1/2})/Cl(^2P_{3/2})$ distributions shown in the bottom panel of Fig. 4 is in reasonable agreement with experiment. By comparison, the adiabatic limit predicts primarily $Cl(^2P_{1/2})$ in contrast to observation. The overall $Cl(^2P_{1/2})/Cl(^2P_{3/2})$ branching is consistent with the statistical prediction despite clear evidence at the correlated level for non-statistical behavior and demonstrating the advantage of correlated measurements. Both exhibit fluctuations around a similar average value although the variation in the experimental data is considerably larger. Since the individual atomic contributions to each molecular state (Table 3) do not show significant variability, the diabatic prediction, which represents a linear combination of these values, is not expected to exhibit large fluctuations in the product branching ratios. The v'-dependent $O(^3P_J)$ distributions are shown in Fig. 5. The experimental values (top panel) again exhibit greater fluctuations than the diabatic model. Interestingly both experiment and the diabatic model on average show significantly higher yields for the $O(^3P_1)$ and $O(^3P_0)$ products than predicted by the statistical (strong coupling) limit. However, the increased yield of $O(^3P_0)$ from $v' = 3$ to $v' = 8$, due to an increase in the $Cl(^2P_{1/2}) + O(^3P_0)$ channel over this range of v', is not well reproduced.

A better comparison between experiment and theory, both from the standpoint of experimental confidence in the values and reflecting an increased level of detail, involves considering the $Cl(^2P_{1/2})/Cl(^2P_{3/2})$ branching fractions for each $O(^3P_J)$ state which are shown in Fig. 6. As discussed previously, these values are derived from the relative intensities of features associated with the formation of $Cl(^2P_{1/2})$ and $Cl(^2P_{3/2})$ in a single image and are therefore relatively insensitive systematic errors. The absence of the $Cl(^2P_{1/2})$ formed in coincidence with $O(^3P_0)$ is consistent with the diabatic prediction. This is not surprising given the lack of contribution from this atomic channel to any of the dissociative states considered in

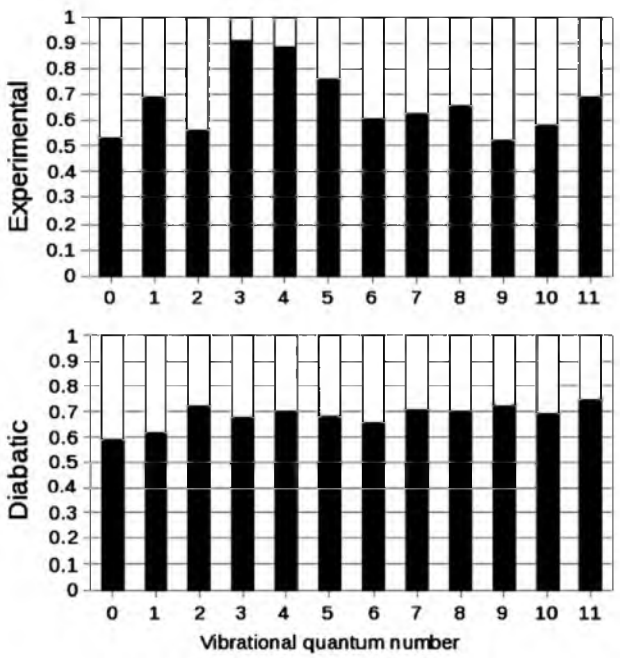

Fig. 4 Overall $Cl(^2P_{3/2})$ (dark) and $Cl(^2P_{1/2})$ (white) branching ratios as a function of $A\ ^2\Pi_{3/2}$ vibrational level. The results from experiment and the diabatic limit model, are shown in the top and bottom panels respectively.

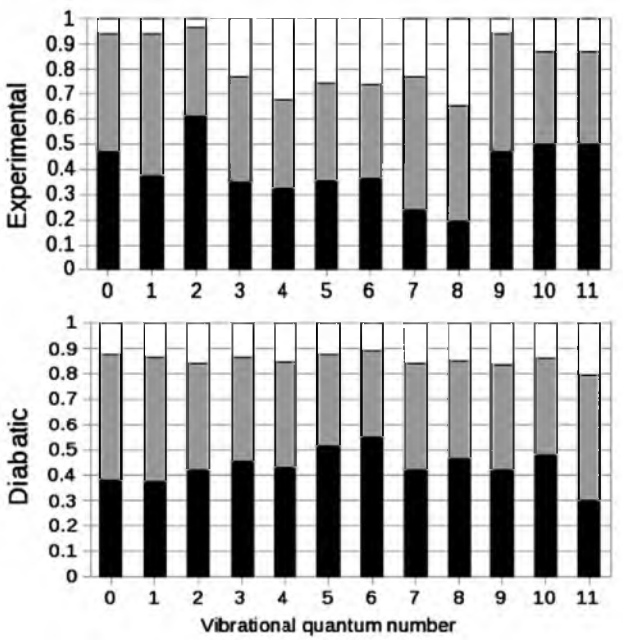

Fig. 5 Overall $O(^3P_2)$ (black), $O(^3P_1)$ (grey), and $O(^3P_0)$ (white) populations for each as a function of $A\ ^2\Pi_{3/2}$ vibrational level. The results from experiment and the diabatic limit model are shown in the top and bottom panels respectively.

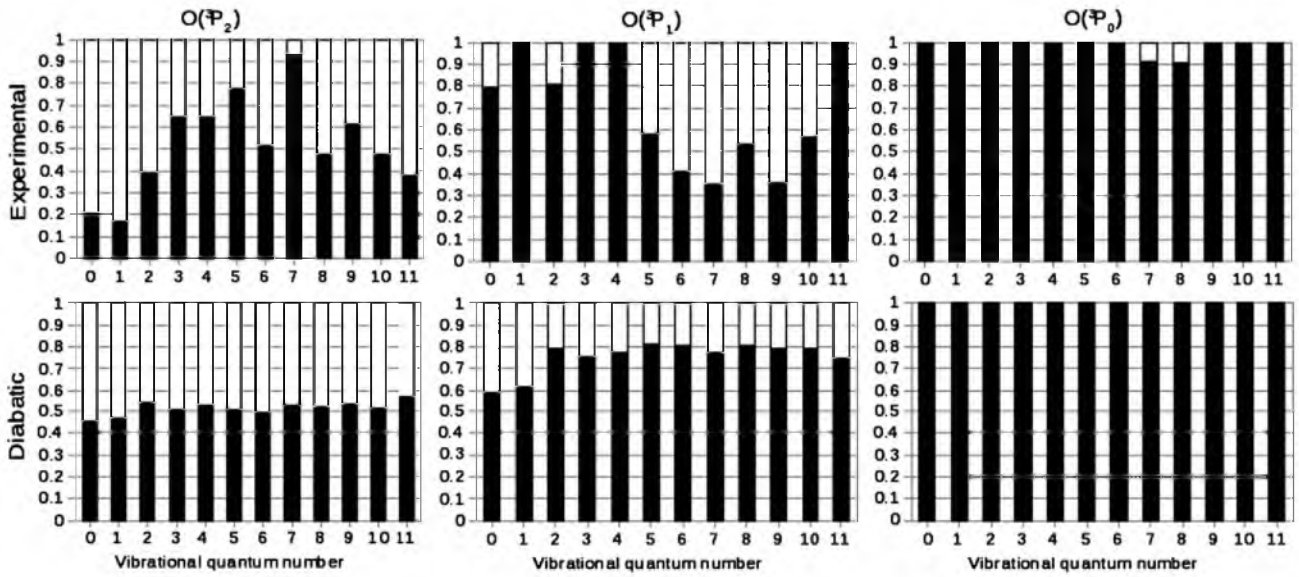

Fig. 6 $Cl(^2P_{3/2})$ and $Cl(^2P_{1/2})$ branching ratios for each oxygen fine-structure state as a function of $A\ ^2\Pi_{3/2}$ vibrational level. The results from experiment and the diabatic limit model are shown in the top and bottom panels respectively.

the model. The experimental data exhibit clear trends in the $Cl(^2P_{1/2})/Cl(^2P_{3/2})$ branching, however, which are not reproduced by the diabatic model. These differences, specifically the increase in the $Cl(^2P_{1/2})$ between $v' = 4$ and $v' = 10$ in coincidence with $O(^3P_1)$, is inconsistent with the diabatic model. We also note that several fine-structure states are observed with populations that exceed their partial contributions to any dissociative states. These values are written in bold italic in Table 1. The fact that these observations cannot be achieved by any set of the potentials considered in the model, including the $1\ ^4\Sigma^+$ state, is clear evidence that exit channel coupling must play a role.

In an effort to assess the role of exit channel coupling we have performed coupled channel calculations, taking into account all 9 $\Omega = 3/2$ molecular potentials that correlate with the $Cl(^2P) + O(^3P)$ atomic limit (see, *e.g.* Table 3 in ref. 18). For this purpose we employed the *ab initio* potentials of Toniolo *et al.*[12] We also included the small corrections to the *ab initio* potentials that were introduced to improve agreement with available experimental data.[12,33] We neglect the effects of rotation and only consider the R-independent atomic spin orbit coupling. This coupling is diagonal in the atomic fine-structure basis:

$$|J_{Cl}\Omega_{Cl}\rangle|J_O\Omega_O\rangle, \tag{8}$$

where J_i (i = Cl, O) are the total electronic angular momentum quantum numbers for the atoms, and Ω_i the projections on the interatomic axis. The diagonal atomic spin–orbit coupling matrix elements are given by

$$\tfrac{1}{2}A_{Cl}[J_{Cl}(J_{Cl}+1) - L_{Cl}(L_{Cl}+1) - S_{Cl}(S_{Cl}+1)] + \tfrac{1}{2}A_O[J_O(J_O+1) - L_O(L_O+1) - S_O(S_O+1)], \tag{9}$$

where the atomic orbital angular momentum quantum numbers for Cl and O are $L_{Cl} = L_O = 1$, the atomic spin quantum numbers $S_{Cl} = 1/2$ and $S_O = 1$, and the spin–orbit coupling constants are $A_{Cl} = -(2/3)882.4\ cm^{-1}$ and $A_O = -227/3\ cm^{-1}$. The coupling in the molecular basis arises from the transformation of the atomic to the molecular basis. This transformation was discussed in ref. 18. Briefly, it is based on the general treatment of the photodissociation of diatomic molecules as presented by Singer *et al.*[34,35] Molecular states of the same symmetry are defined by considering the long range quadrupole-quadrupole interaction, as detailed in ref. 31 and 32, where it was shown that for two P state atoms the asymptotic molecular states can be characterized by the total orbital angular momentum quantum number L, in addition to the usual Hund's case (a) quantum numbers Λ, S, and Σ. The expression for the basis transformation elements $\langle J_{Cl}\Omega_{Cl}J_O\Omega_O|(L)\Lambda S\Sigma\rangle$ is given by eqn (5) of ref. 32.

The branching ratios were computed in the Fermi golden rule (FGR) approximation. In this approximation the rate of decay of a v' vibrational level of the $A\ ^2\Pi_{3/2}$ electronic state into the (J_{Cl}, J_O) atomic product channel, due to coupling between the A state with repulsive predissociating electronic state $|n\rangle$, is proportional to the partial linewidth

$$\Gamma^{(n)}_{v';J_{Cl}J_O} = \frac{2\pi}{\hbar}\sum_{\Omega_{Cl}+\Omega_O=\Omega} |\langle A^2\Pi_{3/2}(v')|\hat{H}_{A,n}|\Psi_{J_{Cl}\Omega_{Cl}J_O\Omega_O}\rangle^2, \tag{10}$$

where $\Psi_{J_{Cl}\Omega_{Cl}J_O\Omega_O}$ is the energy normalized continuum wave function computed for photodissociation boundary conditions,[36] for a total energy equal to the energy of the $A^2\Pi_{3/2}$ (v') predissociating level. This level was computed with the sinc-function discrete variable representation method,[37,38] with a A-state potential computed with the Rydberg–Klein–Rees program of Le Roy,[39] taking the required spectroscopic data from Howie *et al.*[10] The continuum wave function was computed with the renormalized Numerov method[40] on a grid extending from $R = 2.4$ to 10 a_0, and the integral was propagated along with the wave function with a method similar to the one described by Gadéa *et al.*[41] For the coupling Hamiltonians $\hat{H}_{A,n}$ we take the spin–orbit

and electrostatic couplings given in Table 3 of ref. 12. The electrostatic interaction between the $A^2\Pi_{3/2}$ state and the $3^2\Pi_{3/2}$ state (112 cm^{-1}) and the spin–orbit interaction between these states (12 cm^{-1}) are combined as $\sqrt{112^2 + 12^2}$ cm^{-1}.[12] The couplings were only given for the crossing distances between the A state and the predissociating states, so we take them as R-independent. The branching ratios were computed by taking an incoherent sum of the partial linewidth for all predissociating states, and normalizing the result to one.

The results of the coupled channels calculations are shown in Table 1 (the rows labeled "coupled channel"). Clearly, there are substantial differences between the coupled channel and diabatic model results, which demonstrates that exit channel coupling cannot be neglected and so the diabatic limit is not reached. We note that the diabatic model predictions based on the potentials of Toniolo *et al.* are very similar to the diabatic model predictions using the potentials of Lane *et al.* even if the former couplings are adjusted to best reproduce the reported predissociation lifetimes. We can compare the coupled channel model and diabatic models by computing root-mean-square (rms) differences between the correlated branching rations for each individual vibrational levels v'. We find that although the overall the coupled channel result is marginally better, the rms difference with experiment rounded to two digits is 0.11 for both methods. However, the difference between the diabatic model and the coupled channel calculation is substantial (rms = 0.076). Coupled channel calculations where we replaced four of the *ab initio* potentials by the corresponding Lane *et al.* potentials and couplings that were optimized to reproduce the predissociation lifetimes resulted in a worse agreement with the observed correlated branching ratios (rms = 0.16).

From these results we conclude that the exit channel couplings have a large effect on the fine-structure branching ratios. This means that the correct R-dependence of the spin–orbit coupling will be required to explain the observed results. It is also likely that more accurate long range potentials are required to obtain quantitative agreement. In summary, progress towards a detailed understanding the dissociative dynamics of ClO is encouraging but differences between experiment and theory outside the estimated experimental error bounds remain and further work to resolve these outstanding issues is warranted.

Acknowledgements

The authors wish to thank Andrew Orr-Ewing for sharing *ab initio* results and Robert Le Roy for assistance with implementation of BCONT. Support for this project was provided by the Robert A. Welch Foundation (Grant A-1402). The authors acknowledge the support of the Texas A&M University Center for Atmospheric Chemistry and the Environment (CACE).

References

1 M. J. Molina and F. S Rowland, *Nature*, 1974, **249**, 810.
2 R. R. Garcia and S. Solomon, *J. Geophys. Res.*, 1994, **99** 12937.
3 S. Solomon, R. R. Garcia, F. S. Rowland and D. J. Wuebbles, *Nature*, 1986, **321**, 755.
4 W. Zhou, Y. Yuan and J. Zhang, *J. Chem. Phys.*, 2003, **119** 9989.
5 G. Parlant and D. R. Yarkony, *J. Chem. Phys.*, 1999, **110**, 363.
6 R. A. Durie and D. A. Ramsay, *Can. J. Phys.*, 1958, **36**, 35.
7 J. A. Coxon and D. A. Ramsay, *Can. J. Phys.*, 1976, **54**, 1034.
8 P. W. McLoughlin, C. R. Park and J. R. Weisenfeld, *J. Mol. Spectrosc.*, 1993, **162**, 307.
9 M. Trolier, R. L. Mauldin III and A. R. Ravishankara, *J. Phys. Chem.*, 1990, **94**, 4896.
10 W. H. Howie, I. C. Lane, S. M. Newman, D. A. Johnson and A. J. Orr-Ewing, *Phys. Chem. Chem. Phys.*, 1999, **1**, 3079.
11 I. C. Lane, W. H. Howie and A. J. Orr-Ewing, *Phys. Chem. Chem. Phys.*, 1999, **1**, 3087.
12 A. Toniolo, M. Persico and D. Pitea, *J. Chem. Phys.*, 2000, **112**, 2790.
13 H. F. Davis and Y. T. Lee, *J. Phys. Chem.*, 1996, **100**, 30.
14 P. Zou, H. Kim and S. W. North, *J. Chem. Phys.*, 2002, **116** 4176.
15 H. Kim, J. Park, T. C. Niday and S. W. North, *J. Chem. Phys.*, 2005, **123**, 174303.
16 S. Schmidt, Th. Benter and R. N. Schindler, *Chem. Phys. Lett.*, 1998, **282**, 292.
17 R. Flesch, J. Plenge, S. Kühl, M. Klusmann and E. Rühl, *J. Chem. Phys.*, 2002, **117**, 9663.
18 H. Kim, K. S. Dooley, G. C. Groenenboom and S. W. North, *Phys. Chem. Chem. Phys.*, 2006, **8**, 2964.
19 H. Kim, K. S. Dooley, E. R. Johnson and S. W. North, *Rev. Sci. Instrum.*, 2005, **76**, 124101.
20 D. J. Bamford, L. E. Jusinski and W. K. Bischel, *Phys. Rev. A: At., Mol., Opt. Phys.*, 1986, **34**, 185.
21 D. W. Chandler and P. L. Houston, *J. Chem. Phys.*, 1987, **87** 1445.
22 A. T. Eppink and D. H. Parker, *Rev. Sci. Instrum.*, 1997, **68** 3477.
23 W. Li, S. D. Chambreau, S. A. Lahankar and A. G. Suits, *Rev. Sci. Instrum.*, 2005, **76**, 063106.
24 V. Dribinski, A. Ossadtchi, V. A. Mandelshtam and H. Reisler, *Rev. Sci. Instrum.*, 2002, **73**, 2634.
25 G. A. Garcia, L. Nahon and I. Powis, *Rev. Sci. Instrum.*, 2004, **75**, 4989.
26 G. H. Cady, *Inorg. Synth.*, 1957, **5**, 156.
27 P. L. Houston, G. E. Hall, H. Kim, K. S. Dooley and S. W. North, *J. Chem. Phys.*, 2006, **125**, 133316.
28 The 'betaofnu.exe' program is a result from ref. 27 and is available for download from http://www.cosbkup.gatech.edu/group/Betaofnu.htm.
29 R. J. Le Roy, *Comput.Phys. Commun.*, 1989, **52**, 383.
30 R. J. LeRoy, *University of Waterloo Chemical Physics Report CP-650R*, 2004.
31 M. C. G. N. van Vroonhoven and G. C. Groenenboom, *J. Chem. Phys.*, 2002, **116**, 1954.
32 M. C. G. N. van Vroonhoven and G. C. Groenenboom, *J. Chem. Phys.*, 2002, **116**, 1965.
33 M. Persico, private communication, 2007.
34 S. J. Singer, K. F. Freed and Y. B. Band, *J. Chem. Phys.*, 1983, **79**, 6060.
35 S. J. Singer and K. F. Freed, *Adv. Chem. Phys.*, 1985, **61**, 1.
36 R. Schinke, *Photodissociation Dynamics*, Cambridge University Press, Cambridge, 1993.
37 D. T. Colbert and W. H. Miller, *J. Chem. Phys.*, 1992, **96**, 1982.
38 G. C. Groenenboom and D. T. Colbert, *J. Chem. Phys.*, 1993, **99**, 9681.
39 R. J. LeRoy, *University of Waterloo Chem. Phys. Res. Rep. CP-657R*, 2004, http://leroy.uwaterloo.ca/programs.
40 B. R. Johnson, *J. Chem. Phys.*, 1999, **67**, 4086.
41 F. X. Gadéa, H. Berriche, O. Roncero, P. Villarreal and G. D. Barrio, *J. Chem. Phys.*, 1997, **107**, 10515.

